

# A Satellite Model of Forest Flammability

Marc K. Steininger · Karyn Tabor ·  
Jennifer Small · Carlos Pinto · Johan Soliz ·  
Ezequiel Chavez

Received: 15 March 2012 / Accepted: 6 May 2013 / Published online: 13 June 2013  
© Springer Science+Business Media New York 2013

**Abstract** We describe a model of forest flammability, based on daily satellite observations, for national to regional applications. The model defines forest flammability as the percent moisture content of fuel, in the form of litter of varying sizes on the forest floor. The model uses formulas from the US Forest Service that describe moisture exchange between fuel and the surrounding air and precipitation. The model is driven by estimates of temperature, humidity, and precipitation from the moderate resolution imaging spectrometer and tropical rainfall measuring mission multi-satellite precipitation analysis. We provide model results for the southern Amazon and northern Chaco regions. We evaluate the model in a tropical forest-to-woodland gradient in lowland Bolivia. Results from the

model are significantly correlated with those from the same model driven by field climate measurements. This model can be run in a near real-time mode, can be applied to other regions, and can be a cost-effective input to national fire management programs.

**Keywords** Tropical forest · Fire risk · Drought · Remote sensing · Amazon · Bolivia

## Introduction

### Forest Flammability Models

Models of forest flammability allow a better understanding of fire risk and are sought by national forest agencies to support forest management. Most models use surface-climate data from either in situ measurements or nearby weather stations. The models are typically applied on a daily basis, where the previous day's conditions are modified with the current day's climate. Examples include using the length of time since the last significant rainfall event and a bucket model of soil moisture evaporation (e.g., Nepstad and others 2004; Ray and others 2005; INPE 2011). These parameters are used as indicators of risk, based on underlying assumptions of relationships to the moisture of the available fuels and empirical relationships with the frequency of fire occurrence. Some models include seasonal forecasting, such as that of Chen and others (2011), who use the empirical relationship between sea-surface temperatures and fire activity to forecast fire-season severity, although at a very coarse 5° resolution.

The USFS defines fire risk as the “chance of fire starting, as determined by the presence and activity of causative agents” (NWCG 2013). It defines flammability as the

---

M. K. Steininger (✉) · K. Tabor  
Conservation International, 2011 Crystal Drive, Suite 500,  
Arlington, VA 22202, USA  
e-mail: msteininger@conservation.org

J. Small  
Department of Geography, University of Maryland at College  
Park, 2181 LeFrak Hall, College Park, MD 20742, USA

*Present Address:*  
J. Small  
National Aeronautics and Space Administration Goddard Space  
Flight Center, Mail Code: 614.4, Greenbelt, MD 20771, USA

C. Pinto · J. Soliz · E. Chavez  
Departamento de Geografía, Museo Noel Kempff Mercado,  
Universidad Autonomía Gabriel Rene Moreno, Avenida Irala  
565, Box 2489, Santa Cruz de la Sierra, Bolivia

*Present Address:*  
C. Pinto  
Fundación Amigos de la Naturaleza, Castilla Postal 2241 Santa  
Cruz de la Sierra, Bolivia

“relative ease with which fuels ignite and burn” regardless of the quantity of the fuels and potential ignition sources. Fuel moisture is the most important variable in determining flammability (Byram 1959; Palmer 1965; Keetch and Byram 1968; Bradshaw and others 1984; Albini 1985; Brown 2000). Models used by the National Fire Danger Rating System (NFDRS) of the US Forest Service (USFS) have several components that have been developed based on theory and years of field measurements. A key part of the NFDRS models is the estimation of the moisture exchange and content of fuels of varying sizes, both live and dead, on the forest floor as a means to estimating flammability.

Fuel moisture content varies over time depending on moisture uptake from precipitation and moisture loss from evaporation to the surrounding air. The average moisture content changes more slowly for fuel in the form of large pieces of litter than for small. This variation in exchange rate is described by a time-lag coefficient which varies among size classes. The NFDRS classifies fuel sizes in 1-, 10-, 100-, and 1,000-h time-lag classes. These correspond to fuels with diameters of <0.6 cm, 0.6–2.5 cm, 2.5–7.6 cm, and >7.6 cm (Fosberg 1971, 1977; Fosberg and others 1981).

The fuel class describes the moisture exchange properties of collections of fuel on the forest floor, e.g., foliage and twigs, branches, or tree trunks (Anderson 1982). The finer fuels are 1- and 10-h fuels because their average moisture changes more quickly via exchange with the surrounding air, because of their smaller diameters. The 100-h fuels are medium-sized fuel while the 1,000-h fuels can be large logs, having the slowest rates of change in average moisture.

The probability of ignition (PI) of fuels, as described in the NFDRS model, increases when moisture content is below 15–20 %, depending on the fuel properties and heat of the ignition source (Schroeder 1969; Anderson 1982; Bradshaw and others 1984). A fire is unlikely to spread to fuels with moisture levels of over 20 %. The intensity of a burn also increases when the moisture content of fuels decreases below 20 % (Table 1; Albini 1979; Burgen 1979; Scott and Burgan 2005).

Thus, the PI addresses the relationship between fuel type, moisture, climate, and the likelihood of fuel ignition, accounting for much of the variability in flammability. Other parameters, such as fuel load and wind speed, are used in the NFDRS and other models to describe the likelihood that a fire will spread, and these are used to model fire risk.

#### Satellite Bioclimatology

Satellite observations are commonly used for estimating or modeling the biophysical structure and processes in

**Table 1** Ignition potential for fine fuels versus fuel moisture content, adapted from Albini (1979)

Fuel moisture (%)	Relative ease of ignition
>25	Little or no ignition
20–25	Very little ignition
15–19	Low ignition hazard, campfires become dangerous
11–14	Medium ignitibility, matches become dangerous; “easy burning conditions”
8–10	High Ignition hazard, matches always dangerous; “moderate burning conditions”
5–7	Quick ignition hazard, rapid buildup, “dangerous burning conditions”
<5	All sources of ignition dangerous; “critical burning conditions”

vegetated landscapes. A major application is the use of daily to seasonal observations of canopy cover and climate with ecosystem models, e.g., climatic controls on photosynthesis and respiration, to estimate gross and net primary productivity (e.g., Prince and Goward 1995; Goetz and others 1999; Myneni and others 2002; Running and others 2004). These models can characterize spatial, seasonal, and inter-annual trends in vegetation productivity. Thermal observations from satellites are also used for real-time detection of active fires (Justice and others 2002) and burned-area mapping (Roy and others 2002; Grégoire and others 2003).

The use of satellite data in assessments of forest flammability or fire risk has been more limited. Satellite-derived inputs to risk estimates have mostly been maps of fuel types derived from mapped vegetation classes, or anomalies in seasonal vegetation indices to identify drought occurrences (e.g., Matson and Holben 1987; Illera and others 1996; Burgan and others 2000, Cardoso and others 2003; Chuvieco and others 2004; Goetz and others 2005; Setzer and Sismanoglu 2009; INPE 2013; USFS 2013). Climatic inputs in these models are mostly interpolated from weather station data (e.g., Burgan and others 1997; Heinsch and Andrews 2010; INPE 2013; USFS 2013).

In this paper, we describe the application of satellite bioclimatology to modeling forest flammability. A satellite data-driven model of forest flammability enables near real-time applications; can provide continuous coverage from the site to global scale; and can be applied in areas with poor data from weather stations. We use satellite estimates of rainfall, air temperature, and relative humidity to drive the NFDRS litter moisture model. The satellite model produces estimates of moisture exchange and average content on a daily basis at a 5-km resolution. Our model produces outputs of fuel moisture for the 10-, 100-, and 1,000-h time-lag classes. Our study is conducted in a range

of tropical forest along a precipitation gradient in Bolivia. We study this area because of the importance of forest fire there, the need for such models to assist forest management, and the lack of a large network of ground-based weather stations. However, the methodological approach should be applicable to other forest ecosystems.

A transect of permanent field plots in the Amazon and northern Chaco was monitored in the field to validate model inputs and outputs. The transect crosses the Chiquitos region in Santa Cruz, Bolivia and extends from humid forest in southern Amazonia, through semi-deciduous forest and to dry woodland in the northern Chaco (Killeen and others 2006). This area has experienced large inter-annual variability in drought conditions and large wildfires during drier years (Phillips and others 2009; Lewis and others 2011). We compare the satellite-based model of 10-h fuel moisture content with a similar model parameterized with field climate data and with field measurements of moisture content of USFS-standard 10-h fuel sticks. We present the model validation with field measurements and report the modeled temporal and spatial variability of moisture content for the 2003 dry season.

In interpreting the results, we assume that fuel on the forest floor is ignitable and flammable at moisture contents of 20 % or less. We model only forest flammability, which we define as fuel moisture content that is indicative of the likelihood of fire ignition and spread. While flammability is independent of fuel load, we note that fuel load is unlikely to be a limiting factor to fire risk in our study area, based on the relatively high fuel production across the gradient. We model only the 10-, 100-, and 1,000-h fuels. We exclude the finest fuels since their moisture content varies on time-scales shorter than available satellite data. We also do not model live fuels, since they are less important to the initiation and spread of fires in tropical forests, although could be significant sources of fuel for larger fires. The model results can be used to assist fire management policy or can be combined with other information, such as on potential ignition sources and wind, to estimate fire risk.

## Methods

Our overall approach uses satellite data inputs to drive the NFDRS models of fuel moisture content for fuels of different time-lag classes. We apply the model on a daily time step, allowing for daily to weekly applications in assessments and warnings by forest management programs, and necessitated by the frequency of the satellite observations.

We limit our study area and the application of the satellite-based model to the lowlands of Bolivia and the central Amazon (Fig. 1) by applying an elevation mask for areas above 330 m Above Sea Level (ASL), using data

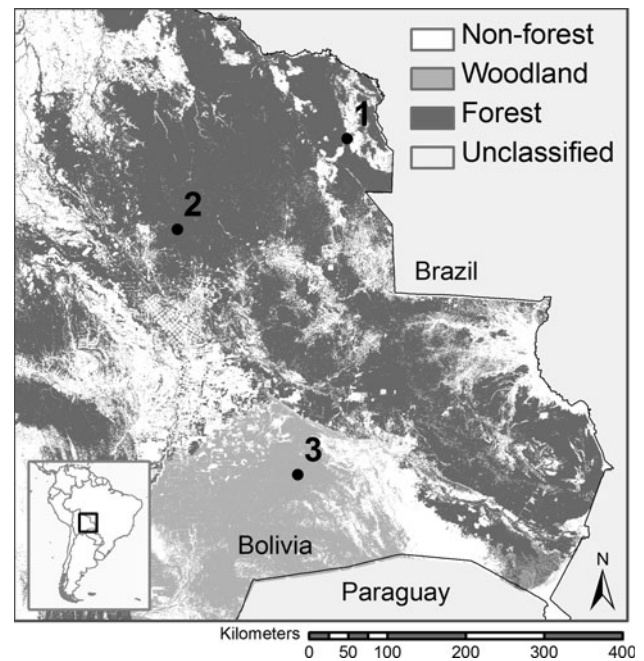


**Fig. 1** Locations of field sites. Sites are 1 Los Fierros, located in the southern portion of Noel Kempff Mercado National Park, 2 La Chonta, located east of Guayaras, and 3 Tucuvaca, located south of San José

from the Shuttle Radar Topography Mission (SRTM) (USGS 2004). A second mask for non-forested areas, based on a 50-percent threshold applied to the tree-cover data in the Moderate Resolution Imaging Spectrometer (MODIS) Vegetation Continuous Fields product, is applied to constrain the model to forested areas (Hansen and others 2003).

## Satellite-Derived Products and Processing

We use satellite-derived data from two separate sources, the MODIS on the Terra satellite and the Tropical Rainfall Measuring Mission (TRMM) Multi-satellite Precipitation Analysis (TMPA) from sensors on multiple satellite platforms. The derived data used in this model are rainfall duration, land surface temperature (LST), and near-surface relative humidity (RH). Rainfall duration is calculated from the TMPA 3B42 product. This product provides three-hourly rainfall rates at 0.25° resolution. The LST is from the 5 km MODIS land product, MOD11B. We generate RH from the bottom layer of the profile in the 5 km MODIS atmosphere product, MOD07L2. MODIS Terra products are generated two times daily and are available in a range of spatial resolutions from 250 m to 1° (~120 km). We chose to only use MODIS Terra data because Terra has a morning overpass, and thus avoiding the generally cloudier observations from afternoon overpasses.

We use rainfall estimates from TMPA because they are the finest resolution, satellite-derived estimates of rainfall available for the global tropics derived from combined measurements of infrared and microwave radiation (Hirpa and Gebremichael 2010). TMPA measures tropical and sub-tropical rainfall with a real-time processing system that combines passive microwave (PM) data from sensors on various low earth orbit (LEO) satellites and infrared (IR) data from the international constellation of geosynchronous earth orbit satellites. These data sources are calibrated and combined to produce the 3B42RT product (Kummerow and others 2000; Huffman and others 2007). TMPA also produces a post-real-time precipitation product, 3B42, that is calibrated with the TRMM Combined Instrument (TCI) estimate and with rain-gage observations from both the Global Precipitation Climatological Center (GPCP) and the Climate Assessment and Monitoring Systems (CAMS) and is available at the end of every month (Huffman and others 2007). Three-hourly precipitation rates are reported for 0.25° cells, approximately 28 km at the equator, from 50° South to 50° North latitude.

The 3B42RT product is available on the website (<ftp://trmmopen.gsfc.nasa.gov/pub/merged/mergeIRMicro>) about 9 h after observation time and is considered an experimental product. The post-real-time product is computed within a few days after the end of the month and is available on the website (<http://mirador.gsfc.nasa.gov/cgi-bin/mirador/presentNavigation.pl?project=TRMM&tree=project>). The 3B42 version 6 is a research-quality TMPA product, which is better correlated to rain-gage data than the 3B42RT product, as expected since the product post-processing calibrates the estimates with rain-gage data. The 3B42RT product tends to significantly overestimate rainfall when there is high rainfall accumulation (e.g., a large rainfall event) and underestimates rainfall in cool, dry climates/seasons (Katsanos and others 2004; Ebert 2005; Dinku and others 2007; Huffman and others 2007). Validation of TMPA, based on four locations globally, shows an error range of  $-3$  to  $+15$  % when compared to ground rainfall data (Wang and Wolff 2010). For both products, we convert three-hourly rainfall rate to rainfall duration in hours by assuming if there is greater than 0.05 mm of rainfall in a 3-h period, there has been a 3-h-long rainfall event. Therefore, rainfall duration is summed in 3-h intervals during a 24-h period. Both the real-time (3B42RT) and post-real-time (3B42) TMPA rainfall data sets can be used in the model. The 3B42 is used for historical analysis and the 3B42RT is used for real-time model runs. The model results presented in this paper were generated using the 3B42 product.

LST estimated from satellites is a measurement of the thermal radiation emitted from both the ground and

overlying vegetation and the proportion from each varies with canopy cover. The LST data in this study are from the daily MODIS MOD11B1 land surface temperature product (Wan and Li 1997). This product is created from a physics-based algorithm that uses day-time and night-time observations in seven MODIS bands for simultaneously retrieving surface temperatures and band-averaged emissivities for all land cover types (Wan and Li 1997; Wan 2009). LST from MOD11B1 has been found to have an RMS of under 2 °C for a set of MODIS field validation sites, with underestimation in some cases up to 3 °C (Wan and others 2004; Wang and others 2007).

The third model input is RH, reported as water vapor pressure as a percent of pressure at saturation. RH is not a MODIS product, however, it can be calculated from the air temperature and dew point temperature in the MOD07L2 atmospheric profile product. MOD07L2 contains vertical profiles, with 20 atmospheric layers, of air temperature, dew point temperature, and pressure (Seemann and others 2003, 2006). RH can be calculated with equations:

$$VP = 0.611 * \exp(17.27 * (T_{air} - 273)/(T_{air} - 36)) \quad (1)$$

$$SVP = 0.611 * \exp(17.27 * (T_{dpt} - 273)/(T_{dpt} - 36)) \quad (2)$$

$$RH = SVP/VP \quad (3)$$

where VP is vapor pressure in kPa, SVP is saturated vapor pressure in kPa,  $T_{air}$  is air temperature in degrees Kelvin,  $T_{dpt}$  is dew point temperature in degrees Kelvin and RH is relative humidity (Monteith and Unsworth 1990).

Both LST and RH are from MODIS Collection IV and are acquired from the morning overpasses of the Terra satellite. They are re-sampled to a 5-km resolution, and MOD11B1 is a delivered as a level-3 tiled product while MOD07L2 is a level-2 orbital-swath product.

The MODIS products have areas of no data because of cloud cover and gaps in between swaths that vary by day. Both products include a mask that is a best estimate of cloud cover derived from the MODIS cloud cover product, MOD35. We spatially interpolate under cloudy areas and gaps to create continuous fields of daily LST and RH data. Cloud-free observations are sought in the 32 cardinal directions around each cloud-mask pixel. The search increases in distance until four cloud-free observations are found. The source pixel is then assigned the distance-weighted average value of the four nearest cloud-free observations. For MOD07L2, interpolations are applied independently to  $T_{air}$  and  $T_{dpt}$  prior to calculation of RH. Calculations and interpolations are done for all lowlands areas, but results are reported only for forest and woodland areas.

Fuel Moisture

The NFDRS models litter moisture exchange for four time-lag classes: 1-, 10-, 100-, and 1,000-h, corresponding to fine fuels, i.e., fallen leaves and small twigs, and coarser fuels with diameters of 0.6–2.5 cm, 2.5–7.6 cm, and >7.6 cm, respectively (Fosberg 1971, 1977; Fosberg and others 1981; Bradshaw and others 1984; Cohen and Deeming 1985). Our model uses the NFDRS equations to estimate moisture content of the latter three fuel classes: 10-, 100-, and 1,000-h.

Moisture Equilibrium

For all fuel time-lag classes, a common moisture equilibrium content (Me) for the current day’s LST and RH is calculated. The equation used depends on the input RH. The resulting Me is the average moisture content of the fuel when in equilibrium with the surrounding air.

For  $RH < 10\%$  :

$$Me = 0.03229 + 0.281073 * RH - 0.000578 * RH * LST \tag{4}$$

For  $10\% < RH < 50\%$  :

$$Me = 2.22749 + 0.160107 * RH - 0.014784 * RH * LST \tag{5}$$

For  $RH > 50\%$  :

$$Me = 21.0606 + 0.005565 * RH - 0.00035 * RH * LST - 0.483199 * RH \tag{6}$$

Boundary Moisture

When applied at a daily time step, Me is combined with daily rain duration (PPTD) to calculate the average moisture at the boundary (Mb), or surface of the fuel in the 100- and 1,000-h time class, over the 24-h period:

Mb for 1,000-h fuels :

$$Mb_{1000} = (PPTD * Me + PPTD * (2.7 * PPTD + 76))/24 \tag{7}$$

Mb for 100-h fuels :

$$Mb_{100} = (PPTD * Me + PPTD * (0.5 * PPTD + 41))/24 \tag{8}$$

Boundary moisture for the 10-h time-lag class is calculated in two time intervals at 0–14 h and 15–24 h. Boundary moisture calculated for the 10-h fuels for the first 15 h is:

$$Mb_{10_{period1}} = ((15 - PPTD_{period1}) * Me + (2.7 * PPTD_{period1} + 76))/15 \tag{9}$$

Boundary moisture calculated for the 10-h fuels for latter 9 h:

$$Mb_{10_{period2}} = ((8 - PPTD_{period2}) * Me + (2.7 * PPTD_{period2} + 76))/9 \tag{10}$$

Moisture Exchange

For 100- and 1,000-h fuels, a unique moisture exchange (Mex) over the 24-h period is calculated to estimate change from the previous day’s moisture content, or initial moisture content (Mi). The form of the equation is common:

$$Mex = Mb - Mi * (1 - X * (\exp(-24/L))) \tag{11}$$

where X is a constant specific to each class and L is the time-lag class in hours. The constant X is 0.87 when L is 100 and 0.82 when L is 1,000. Similar to boundary moisture, moisture exchange for 10-h fuels is calculated in two time steps:

$$Mex_{10_{period1}} = Mb_{10_{period1}} - Mi * (1.0 - 1.1 * \exp(-1.6)) \tag{12}$$

$$Mex_{10_{period2}} = Mb_{10_{period2}} - MC_{10_{period1}} * (1.0 - 0.87 * \exp(-0.8)) \tag{13}$$

Moisture Content

Moisture content (MC) for 100- and 1,000-h fuels is therefore:

$$MC = Mi + Mex \tag{14}$$

Moisture content for 10-h fuels:

$$MC_{10_{period1}} = Mi + Mex_{10_{period1}} \tag{15}$$

$$MC_{10_{period2}} = MC_{10_{period1}} + Mex_{10_{period2}} \tag{16}$$

where the current day’s moisture content is equal to  $MC_{10_{period2}}$ , the moisture content at the end of the second time period. The model is initiated in the beginning of the calendar year with a starting moisture content of 17 %. We chose this value because the start date is in the middle of the rainy season. This is slightly below the typical range of modeled moisture content, mostly between 20 and 40 %, during the rainy season. This allows the model to increase toward a moisture equilibrium during the wet season without beginning with a saturated value. “Appendix” has a table of all variables to the equations above.

The model currently runs with freeware and code written for a Windows or Unix/Linux environment. It uses HDFLook, a data processing and visualization tool provided by NASA (GES DAAC), and the General Cartographic Transformation Package (GCTP). The model is executed through a Unix emulator or run in shell in a Unix/Linux operating system. All of the code is written in C and automated using shell scripting.

Field Validation

We collected validation data from three field sites in Bolivia: Los Fierros, a humid forest site in Noel Kempff Mercado National Park; La Chonta, a humid forest concession near Guayaros; and Tucuvaca, a transition between Chiquitano dry forest Chacoan woodland in the Kaa-Iya national park near San Jose (Fig. 1). Vegetation composition, structure, and transitions across this ecotone are described in Killeen and others (2006). For each site, instruments are distributed within two paired plots, 200 m apart, each 500 m in length. Each site includes continuous data collection from three temperature and humidity sensors and five rainfall gages. Plots were visited throughout 2003 to download data, measure canopy cover and measure moisture content of standard 10-h fuel sticks used by the USFS. Temperature and humidity sensors used were the HOBO data logger and rain gages were the RAINWISE (Onset 2012, Rainwise 2012). The fuel sticks have a dry weight of 100 g, and moisture was measured by weighing the sticks and subtracting the dry weight.

We compare the satellite model to the same model driven with field climate measurements and to measurements of the moisture content of 10-h fuel sticks. The satellite model estimates were extracted from a single cell, rather than an average of a set of cells, due to the coarse resolution of the satellite-derived data compared to the field plot measurements. The field model is continuous because of the climate data loggers, while the fuel moisture measurements were made only on certain days during field visits. We do not conduct a validation of the climate products themselves, as there are numerous studies in progress by the MODIS and

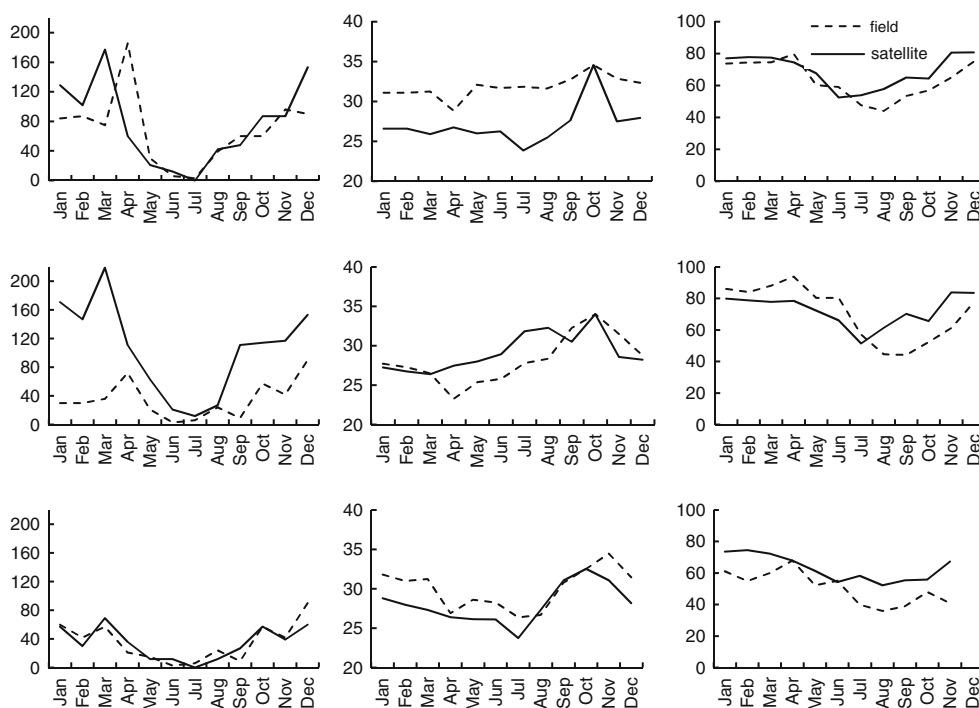
TMPA programs. We do nevertheless report on the trends of these satellite-derived products compared to our field estimates and note the most important errors relevant to the model outputs. MODIS Land surface product has an accuracy better than 1 °C (Wan and others 2004).

Results

Climate Inputs

Estimates of seasonal trends among all three satellite-derived climate variables show agreement with field data, although with biases in some seasons and sites (Fig. 2). For example, the field data for rainfall in the La Chonta site are much lower than estimates from TMPA. There is a general underestimation of LST from the satellite sources, by 5–7 degrees, in the northern Los Fierros site that is not observed in the southern two sites. Satellite estimates of RH showed the closest fit to field measurements, although at times were overestimated by 7–12 %. Our exploration of the daily data showed that most days with rain were reported by the TMPA 3B42 product, with few false positives. Satellite estimates of daily total rainfall were sometimes 40 % or more than the field estimates. However, this was mostly on days with large amounts of rain in which the field instruments were most likely to become clogged with leaves. The satellite estimates of both LST and RH show daily dynamics similar to those in the data from the field measurements, although at times with biases noted above.

**Fig. 2** Field versus satellite-estimated climate inputs to the model: PPT left column, LST center column, Rh right column. PPT is rainfall duration, in hours per month; LST is monthly average of land surface temperature measured during the afternoon satellite overpass, in degrees Celsius; Rh is monthly average of relative humidity measured during the afternoon satellite overpass, in percent. Top row is Los Fierros, middle row is La Chonta, bottom row is Tucuvaca



Satellite-derived RH has high variability over one to several days (Fig. 3). It peaks after rainfall events and rapidly declines over the following 2–3 days. LST shows similar variability at the daily level, although is less-clearly related to rainfall. The dry season is characterized by RH values of around 70 % or lower, as opposed to around 80 % during the wet season. LST shows no clear trend among seasons or sites, while RH indicates longer dry seasons as one moves south in the study area.

### Satellite and Field Models of Moisture

A regression of the field model versus the field measurements, forced through the intercept, produces a slope of 0.62 ( $r^2 = 0.64$ , RMSE = 16.2, df = 22). Removing two potential outlier values, which had measured moisture levels above 60 %, only modestly increased the slope while reducing the correlation (slope = 0.70,  $r^2 = 0.58$ ). The slope and correlation between the satellite-modeled 10-h

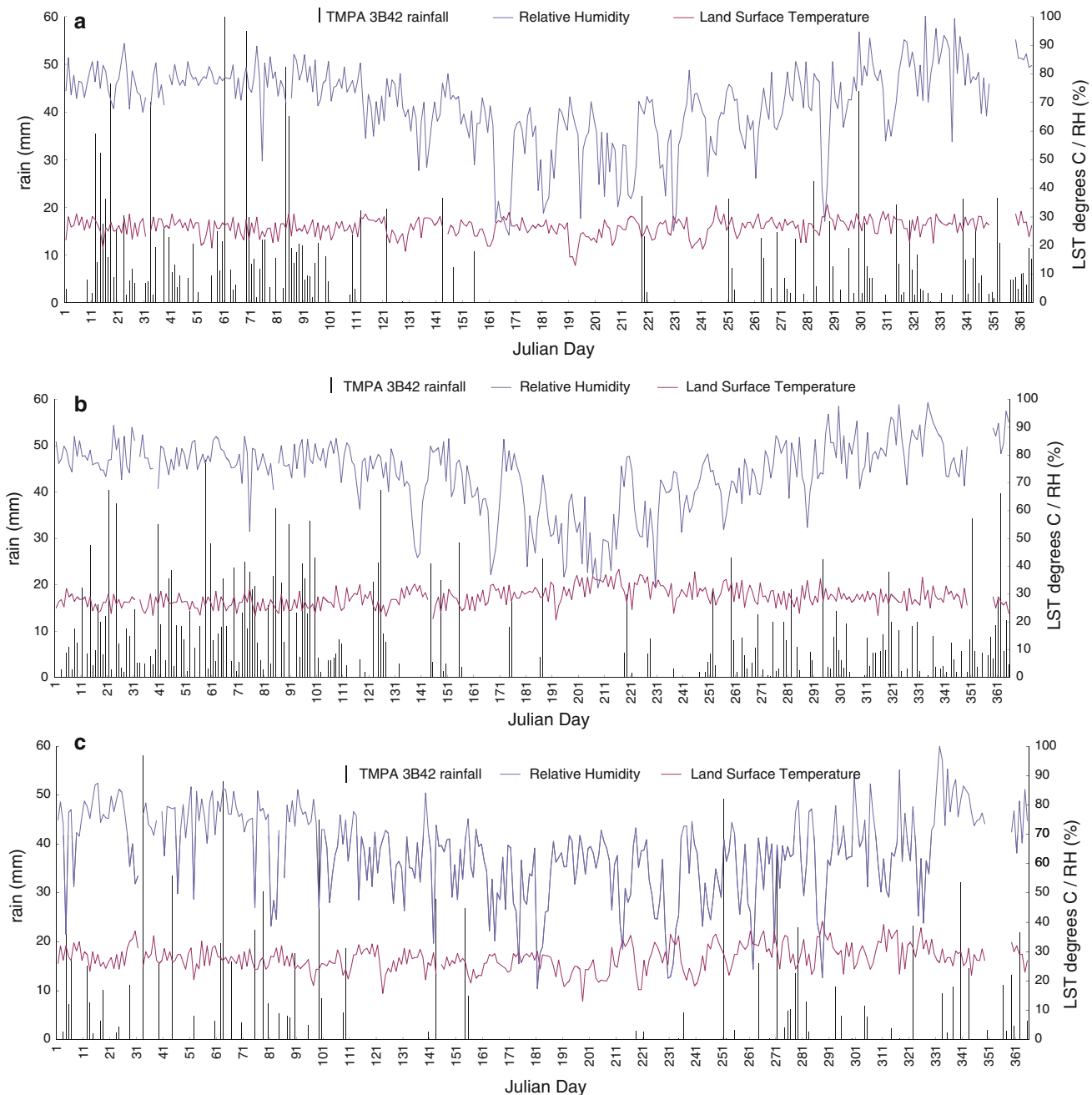


**Fig. 3** Satellite-based inputs to the fuel moisture model for the grid cells over the three field sites: daily precipitation (PPT), derived from the post-processed TMPA 3B42 product; daily land surface

temperature (LST), derived from morning MOD11A2; and daily relative humidity (RH), derived from morning MOD07B1. All data are from 2003. *Top*: Los Fierros; *middle*: La Chonta; *bottom*: Tucuvaca

moisture and the field measurements, also forced through the intercept, are similar to those for the field model (slope = 0.69,  $r^2 = 0.64$ , RMSE = 18.1,  $df = 22$ ). Removing the same two potential outliers produced a slope closer to unity with a similar correlation (slope = 0.86,  $r^2 = 0.64$ ). All of these regressions are significant at the 0.001 level. Without forcing through the intercept, each regression yielded flatter slopes, positive intercepts with larger errors, and lower correlations.

A test of the correlation between the satellite and field models was also conducted (Fig. 4). The regression with the 10-h satellite model as dependent versus the field model, forced through the intercept, produces a slope of 1.03, with a standard error of the slope of 0.03 ( $r^2 = 0.60$ , RMSE = 16.8,  $df = 1062$ ). A regression of satellite model versus field model for 100-h moisture has a slope of 1.05 ( $r^2 = 0.92$ , RMSE = 5.3,  $df = 1062$ ), and that for 1,000-h moisture has a slope of 1.07 ( $r^2 = 0.85$ , RMSE = 9.6,  $df = 1062$ ). All of these regressions are significant at the 0.0001 level.

#### Temporal and Spatial Patterns of Moisture Content

For both the satellite model and the field model, estimates of 10-h moisture content vary closely with RH, with added spikes, and declines over a few days following rainfall events (Fig. 5 compared with Fig. 3). Both humid forest sites, Los Fierros and La Chonta, maintained moisture contents of around 20 % or above through the wet season. Toward the beginning of May, Julian day 115, moisture begins to reach 15 %. Dry season moisture is mostly below this level, except after rains, until the end of September, Julian day 275. The estimates for the Tucuvaca site are similar yet a few percentage points lower throughout the year. This is enough to increase the number of days with moisture below 15 %.

The satellite model follows the field model closely except for the latter period in La Chonta, where the satellite model overestimates moisture. The satellite model also

slightly overestimates moisture throughout the year at Tucuvaca. In both Tucuvaca and the latter period in La Chonta, overestimation of moisture content by the satellite model is associated with overestimation of RH. The satellite model also appears to overestimate the peak moisture after rains, although in either case moisture declines just as quickly over the following days.

The temporal patterns for the 100- and 1,000-h fuel classes are similar to those for the 10-h class, although with lower peaks and slower declines (Fig. 6). As a result, for most days 100-h fuel moisture is 2–5 % higher and 1,000-h fuel moisture is 5 to 15 % higher than that of 10-h fuel. Thus, there periods a few days after rains when 10-h moisture is below 15 or 20 % while that for the 100- and 1,000-h fuel is not. This is less so in the drier Tucuvaca site.

The spatial patterns of moisture over a given dry season month, such as September, have the expected regional trend of drying to the South and East. The moisture trends are altered by frequent rainfall over various parts of the region, and this is most pronounced for the 10-h fuel class. An example of these trends can be seen in Fig. 7. The eastern Amazon, i.e., the north-eastern part of the study area, shows a drying trend over the first 2 weeks of September. After a large rainfall early in the third week, the moisture content of all three fuel classes increased. Conditions on the fourth week returned to those similar to week two or drier. Rainfall among the three field sites can be seen in Fig. 3, from September 7, Julian day 250, onwards.

An example of daily trends for September 12–15, Julian days 285–288, can be seen in Fig. 8. On day 285, most of Bolivia's forests were flammable, i.e., had fuel moisture levels below 15 %. Rains on day 285 increased the moisture content modeled for day 286, and moisture again decreased over the following 2 days. On day 287, the entire eastern half of the Bolivian lowland forests was flammable, and on day 288 the western forests were as well.

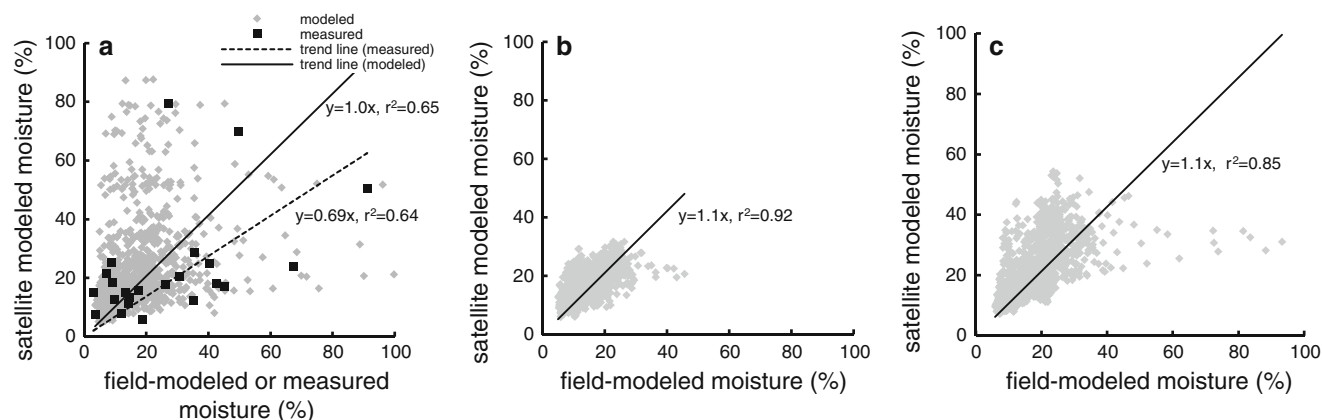


**Fig. 4** Daily 10-h moisture content estimates from the field model, estimates from the satellite model, and measurements of 10-h fuel sticks in the three field sites. *Top*: Los Fierros; *middle*: La Chonta; *bottom*: Tucuvaca

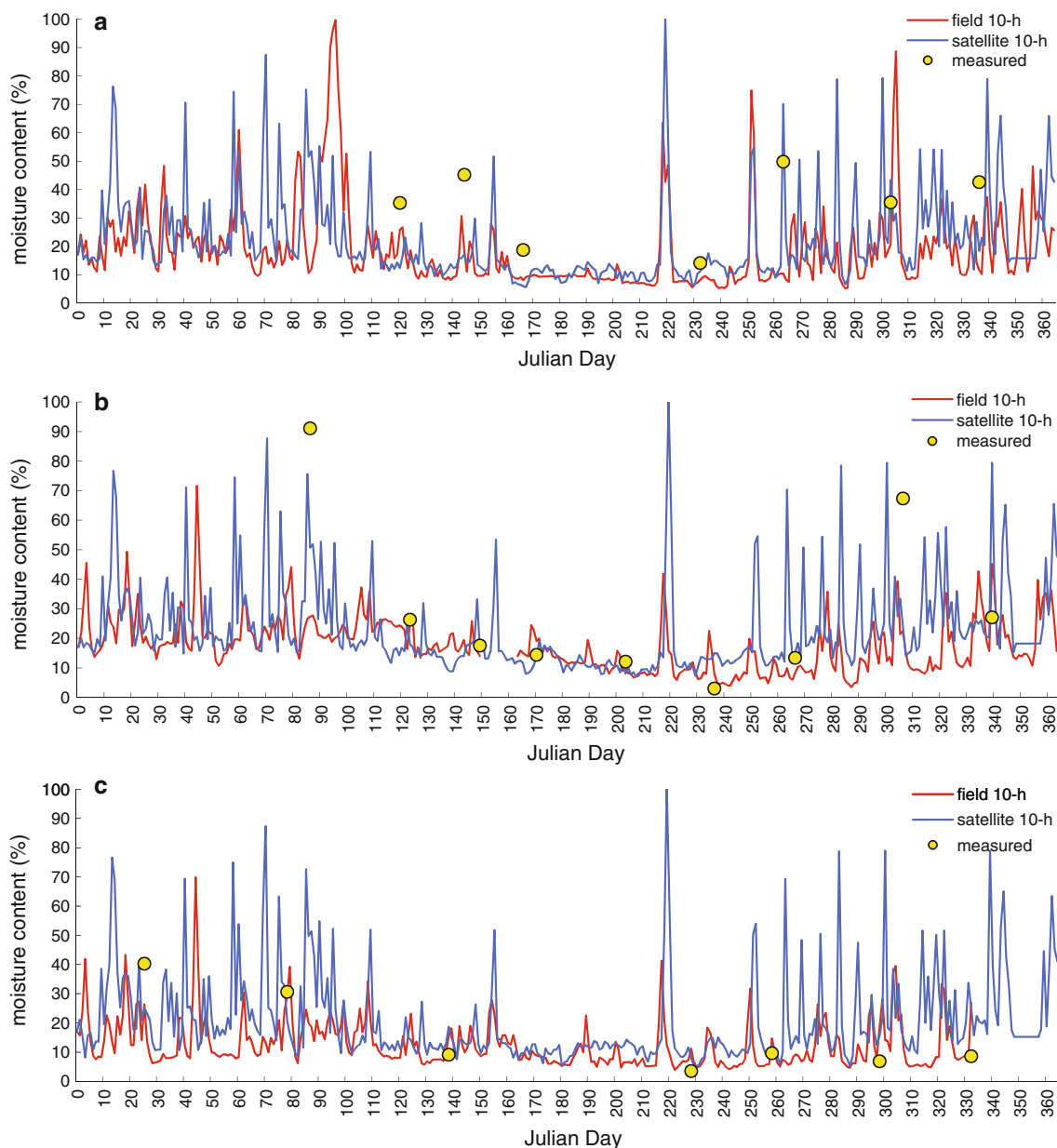


**Fig. 5** Estimates of fuel moisture from the satellite model versus the field model for 10-, 100-, and 1,000-h fuel classes, with field measurements of moisture for 10-h fuels. Data are aggregated from all three field sites

## Discussion

A comparison of the field-based estimates of climatic inputs to those in the satellite-derived products used in the model is revealing. We found biases in both LST and RH. The RH biases are of greater concern because of its importance to the models, and the tendency to overestimate should lead to overestimation of fuel moisture. Also of concern are biases in rainfall, although there are difficulties in validating this in the field. First, instrumental errors in the field data, i.e., leaves clogging the rain gages in between field visits, are difficult to avoid in forested areas. Second, rainfall can have high local

variability, and estimates from one or a few points can be expected to vary greatly from those for coarse cells of the TMPA. More appropriate would be a large network of rain gages spread over the cell's land area, and this is beyond the scope of this study and more appropriately conducted by the TRMM research team.

Only the 10-h models can be compared to field measurements given the data collected. Among the fuel time-lag classes, moisture of 10-h fuels is expected to be most difficult to model because moisture varies more rapidly, is more dependent on when measurements are made during the day, and is very dependent on precipitation, which is

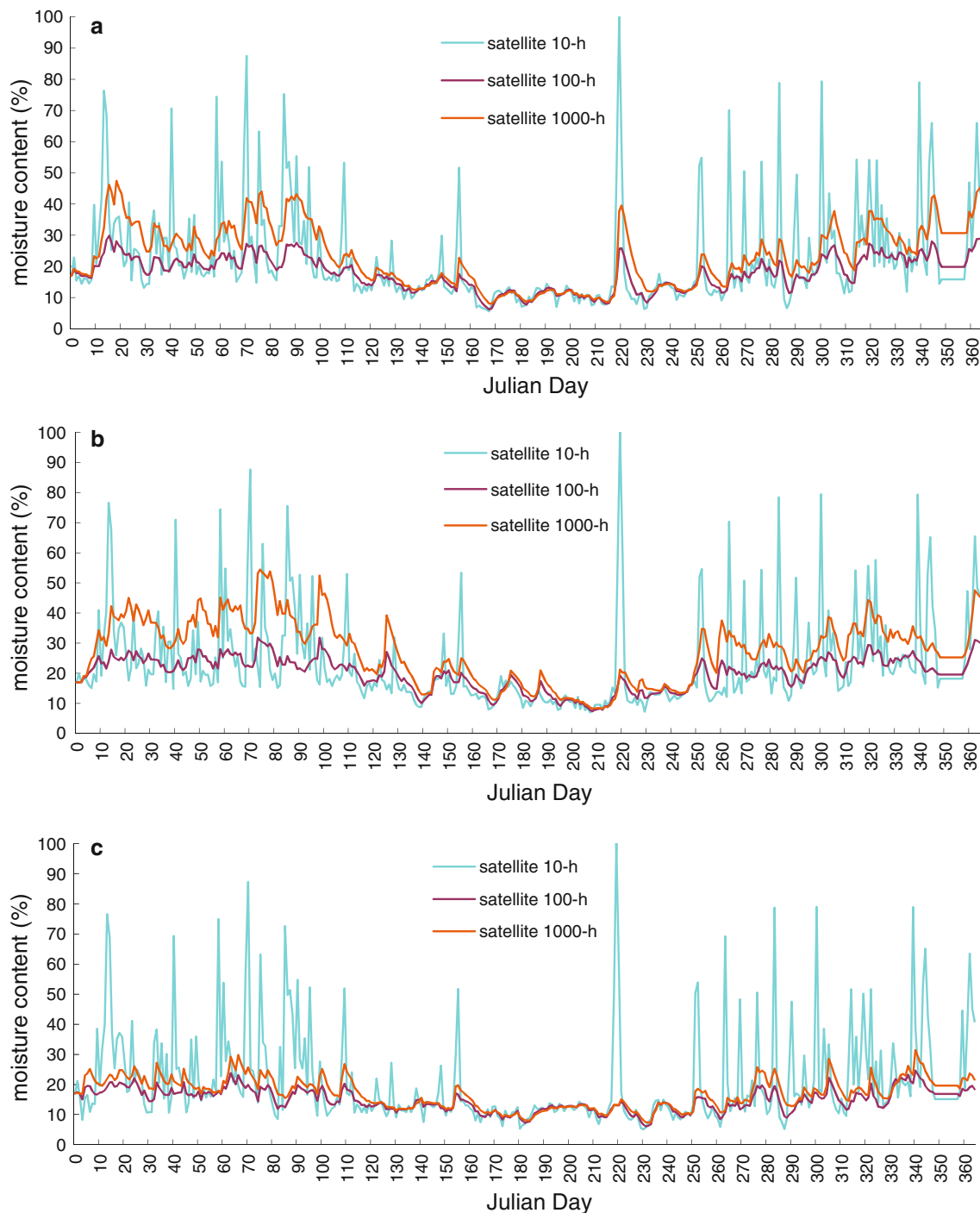


**Fig. 6** Daily estimates of fuel moisture from the satellite model for 10-, 100-, and 1,000-h fuel classes for the three field sites. *Top* Los Fierros; *middle* La Chonta; *bottom* Tucuvaca

more spatially variable than temperature and humidity yet is the coarsest data input for the satellite model. Both the field and satellite model results were positively correlated with the field measurements. In addition, all slopes were less than one, from 0.62 to 0.86, indicating model underestimation to varying degrees. Differences between the

field or satellite model outputs and measured fuel moisture are mostly associated with differences in rainfall estimates, and both the field and satellite estimates of rainfall are potential sources of error. Also, rainfall was the data input with the coarsest resolution in the satellite model, at 0.25 degrees, and it is difficult to expect a strong

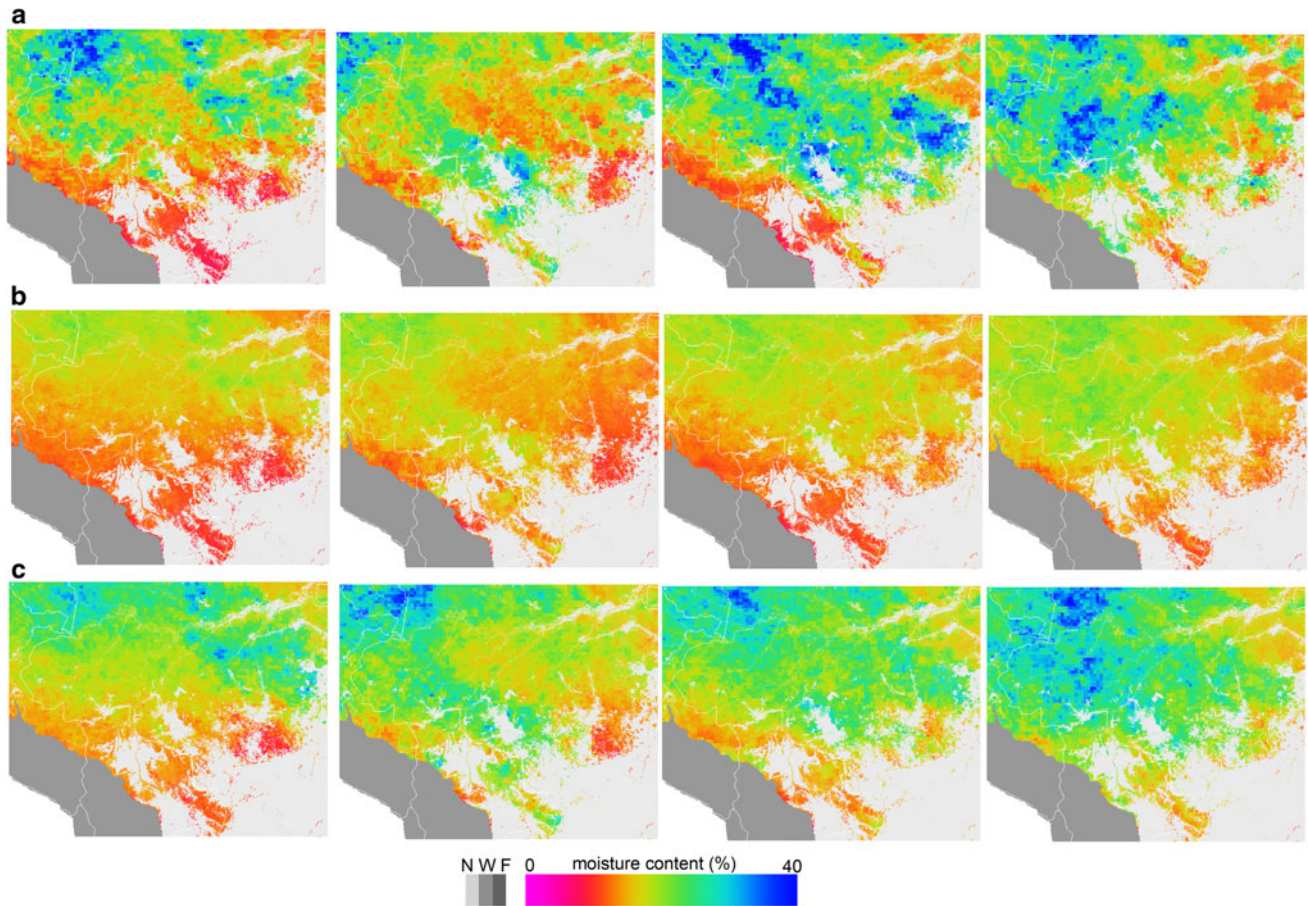


**Fig. 7** Spatial patterns of weekly averages of moisture content from the satellite model. The *top row a* is for the 10-h fuel class, the *middle row b* is for the 100-h fuel class, and the *bottom row c* is for the 1,000-h fuel class. For each row, data are for 09-01-03 to 09-07-03, 09-08-03 to 09-14-03, 09-15-03 to 09-21-03, and 09-22-03 to 09-28-03,

from *left to right*. Areas from *orange to red* indicate moisture values of 15 % and less, indicating increasing flammability for that fuel class. Light gray is non-forest (N), medium gray is forest above 500 m ASL (F), and dark gray areas are water (W). National borders for Brazil, Bolivia, and Peru are in *white*

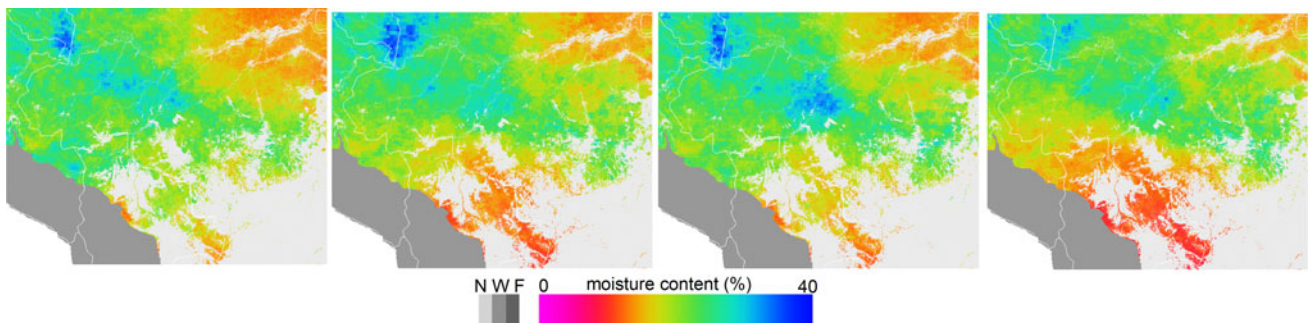


**Fig. 8** Spatial patterns of daily moisture content for the 100-h fuel class from the satellite model. Data are for September 12–15, Julian days 285–288, from *left to right*. Areas from orange to red indicate moisture values of 15 % and less, indicating increasing flammability

for that fuel class. Light gray is non-forest (N), medium gray is forest above 500 m ASL (F), and dark gray areas are water (W). National borders for Brazil, Bolivia, and Peru are in *white*

correlation between point measurements and coarse cells. In addition to rainfall, there were large errors over some periods in the satellite estimates of LST and RH.

Despite low correlation with the measurements and apparent underestimation, there are encouraging results

found in our evaluation. The first is revealed by a comparison of the temporal trends of the 10-h satellite model results and the field measurements during drier periods when flammability is of greatest concern. Of the 23 data points among the three sites when fuel moisture was measured in the field, the

field model is within 10 % of the measured moisture in 12 cases, and the satellite model is within 10 % in 14 cases. Most of the more accurate model outputs are from dry periods critical to wildfire management, especially for the La Chonta and Tucuvaca sites (Fig. 3). The largest errors in the satellite-based estimates were on or after days with substantial rains. These errors in the high-moisture range are of least concern for flammability, since moisture is most likely well above flammable levels, and since it rapidly declines over the following 1–2 days regardless of the peak level, after which it is mostly controlled by RH.

A second encouraging result is found by a comparison of the field and satellite model results. Moisture estimates from both models are strongly correlated for all fuel classes, with correlation coefficients from 0.60 for the 10-h model to 0.92 to the 100-h model. Also, the slopes of the best fits between the two models are all close to unity, from 1.03 to 1.07. Thus, the satellite-based models perform as well as and agrees closely with the field-based models, especially for the coarser fuel classes. However, both 10-h models show significant errors and a tendency to underestimate moisture when compared to field measurements.

The patterns of moisture content for different size classes can be interpreted in the context of the potential spread of a wildfire. For example, on the week of September 1, 10-h fuels were very dry in parts of western-most Brazil. However, 100-h and 1,000-h fuels were on average not sufficiently dry for ignition. Thus, while some smaller pieces of fuel in these forests could ignite, it is unlikely that coarser fuel would burn. The opposite pattern is shown in the south-eastern Brazilian Amazon on the week of September 15. Here, the 1,000-h fuel is dry and the 100-h fuel is close to sufficiently dry for ignition. This is because of low PPTD and RH over the previous several days. However, PPTD on the previous day was enough to increase the 10-h fuel moisture above ignition levels, but not enough to do so for the coarser classes. In this case, it is less likely that a fire would initiate, but if one did it could consume much of the coarser fuels and spread. Among these days, the most flammable conditions were when all three size classes were below the ignition threshold, such as in most of Bolivia on the week of September 1.

We demonstrate here an example of an application of a suite of satellite-derived data to a mechanistic model of fuel moisture. The approach here is a more-direct approach to the estimation of a key parameter for understanding patterns of fire risk than in previous satellite-based applications (e.g., Burgan and others 2000; Cardoso and others 2003; Chuvieco and others 2004; Setzer and Sismanoglu 2009; INPE 2013; USFS 2013). These previous approaches make little use of satellite data, or only do so in other ways. These include mapping of fuel types based on mapped vegetation classes and using deviations in greenness indices as a surrogate for drought conditions. They also include

using climate parameters themselves, such as days-since-last-rain, as surrogates for fire risk. The approach we have applied demonstrates that satellite data are appropriate for applications in a mechanistic model that traditionally is driven with field-based climate data. This is so even despite the substantial improvements that could be made in the accuracy of these satellite-derived climatic inputs.

This model is theoretically applicable to any region, and satellite data for the inputs are available globally. However, local validation should be included in any application. It would be valuable to collect field samples to validate estimates of moisture content of all fuel time-lag classes. Application to mountainous areas may require modification of the model. RH will likely need to be extracted from different levels in the MODIS atmosphere product rather than from one level. Also in mountainous areas, the use of spatial interpolation of daily LST and RH to fill in areas obscured by clouds may be unreliable, and temporal interpolation among days may be more appropriate.

Other approaches to model assessment could include comparison with satellite observations of active fires and burn scars, also available as MODIS products. Further evaluation of the MODIS and GPCP climate products would help this and other projects which use these data in applications. There are currently relatively few validation studies for these products. In addition, these data could be even more useful if further derived products were provided, for example, interpolated estimates and modeled diurnal estimates of LST and RH.

This model addresses only flammability, using fuel moisture content as an indicator, rather than fire risk. The model is applied at a daily time step and intended for management applications over days to weeks. Furthermore, the satellite data do not allow the application of models at an hourly time step, which would be needed to estimate moisture content for the finest fuel class. It is expected that moisture levels of this class vary above and below those in the 10-h class, especially immediately after rain events and rapid changes in humidity.

Flammability is a key parameter for fire risk and these results can be used directly as an input to forest management. Other data could be included to approach fire risk itself. The next most important parameters to include for this would be fuel type and load, wind and ignition sources. Fuel type and load are probably not a constraint on fire risk in this study area, because of high vegetation biomass and litter production, although can be in other areas. Both could be assigned average or seasonal values based on a classification of vegetation types, as done in the US in the NFDRS. A more sophisticated approach could use satellite-derived, seasonal greenness indices to model litter production. Ignition source could be in part modeled from satellite observations of active fires as well as inferences based on maps of agricultural land, towns, and roads. Wind speed could be obtained from networks of

weather station data or satellite sources (e.g., Machado 2000). Likewise, further research on flammability, fire risk, and behavior in tropical forests would be helpful. For example, it is unclear which fuel classes should be most important to model, especially the fine fuels not included in this study. It is also unclear how to best use other data sources to better estimate risk rather than flammability.

The model in its current form can inform forest fire management efforts in the study area, as it is being used by the government of Santa Cruz, Bolivia and NGO partners (GADSC 2013). The model is written in a combination of C/C++ code, shell scripts, and utility programs. It can be installed and executed with no software cost. Currently, the model is running in a near real-time mode for the study area shown and is accessible at <http://firerisk.conservation.org>.

**Acknowledgments** This study was supported by a Grant from the National Aeronautics and Space Administration (NASA Grant # NAG13-02008). We thank Geoffrey Blate for his support in compiling the field data, George Huffman and Louis Giglio for providing expert advice during the development of this model, Tim Killeen and the Museo Noel Kempff Mercado for logistical support, the Fundacion Amigos de la Naturaleza (FAN), the Bolivia Forestry project (BOLFOR), and Wildlife Conservation Society (WCS) for access to field sites.

## Appendix

See Table 2.

**Table 2** Abbreviations and terms in equations

Abbreviation	Description	Unit
L	Time-lag class	Hours
LST	MODIS MOD11B1 land surface temperature	Degrees Celsius
Mb100	Moisture at the boundary (surface) for 100-h fuel	Percent
Mb1000	Moisture at the boundary (surface) for 1,000-h fuel	Percent
Mb10 <sub>period1</sub>	Moisture at the boundary (surface) for 10-h fuel for first 15 h of the 24-h period	Percent
Mb10 <sub>period2</sub>	Moisture at the boundary (surface) for 10-h fuel for final 9 h of the 24-h period	Percent
Mb	Moisture at the boundary (surface)	Percent
MC10 <sub>period1</sub>	Moisture content for 10-h class for first 15 h of the 24-h period	Percent
MC	Moisture content	Percent
Me	Moisture equilibrium content	Percent
Mex10 <sub>period1</sub>	Moisture exchange for 10-h class for first 15 h of the 24-h period	Percent
Mex10 <sub>period2</sub>	Moisture exchange for 10-h class for final 9 h of the 24-h period	Percent
Mex	Moisture exchange	Percent

**Table 2** continued

Abbreviation	Description	Unit
Mi	Initial moisture content	Percent
PPTD	TRMM 3B42 rainfall duration for 24-h period	Hours
PPTD <sub>period1</sub>	TRMM 3B42 rainfall duration for first 15 h of the 24-h period	Hours
PPTD <sub>period2</sub>	TRMM 3B42 rainfall duration for final 9 h of the 24-h period	Hours
RH	Relative humidity calculated from MODIS MOD07 Atmospheric Profiles	Percent
SVP	Saturated vapor pressure	kPa
Tair	Air temperature from MOD07 atmospheric profiles	Degrees Kelvin
Tdpt	Dew point temperature from MOD07 atmospheric profiles	Degrees Kelvin
VP	Vapor pressure	kPa
X	Constant specific to each time-lag class L	Unitless

## References

- Albini FA (1979) Spot distance from burning trees—a predictive model. USDA Forest Service general technical report INT-56. Intermountain forest and range experiment station, Forest Service, US Department of Agriculture, Ogden, Utah, USA
- Albini FA (1985) A model for fire spread in wildland fuels by radiation. *Combust Sci Technol* 42:229–258
- Anderson H (1982) Aids to determining fuel models for estimating fire behavior. USDA Forest Service general technical report INT-122. Intermountain Forest and Range Experiment Station, Forest Service, US Department of Agriculture, Ogden, Utah, USA
- Bradshaw LS, Deeming JE, Burgan RE, Cohen JD (1984) The 1978 national fire-danger rating system: technical documentation. General technical report INT-169. US Intermountain Forest and Range Experiment Station, Forest Service, US Department of Agriculture, Ogden, Utah, USA
- Brown JK (2000) Wildland fire in ecosystems: effects of fire on flora. USDA Forest Service general technical report Gen. Tech. Rep. RMRS-GTR-42-vol 2. Ogden, UT: US Department of Agriculture, Forest Service, Rocky Mountain Research Station, US Department of Agriculture Ogden, UT, USA
- Burgan RE, Andrews PL, Bradshaw LS, Chase CH, Hartford RA, Latham DJ (1997) WFAS: wildland fire assessment system. *Fire Manag Notes* 57(2):14–17
- Burgan RE, Klaver RW, Klaver JM (2000) Fuel models and fire potential from satellite and surface observations. <http://www.fs.fed.us/land/wfas/firepot/fpipap.htm>. Accessed online 8 Apr 2009
- Burgan RE (1979) Estimating live fuel moisture for the 1978 national fire danger rating system. USDA Forest Service research paper INT-226. Intermountain Forest and Range Experiment Station, Forest Service, US Department of Agriculture, Ogden, Utah, USA
- Byram GM (1959) Combustion of forest fuels. In: Davis KP (ed) *Forest fire control and use*, 2nd edn. McGraw-Hill Book Company, New York, pp 113–126
- Cardoso MF, Hurtt GC, Moore B III, Nobre CA, Prins EM (2003) Projecting future fire activity in Amazonia. *Glob Change Biol* 9:656–669

- Chen Y, Randerson JT, Morton DC, DeFries RS, Collatz GJ, Kasibhatla PS, Giglio L, Jin Y, Marlier ME (2011) Forecasting fire season severity in South America using sea surface temperature anomalies. *Science* 334:787–791
- Chuvieco E, Cocero D, Riaño D, Martín P, Martínez-Vega J, de la Riva J, Pérez F (2004) Combining NDVI and surface temperature for the estimation of live fuel moisture content in forest fire danger rating. *Remote Sens Environ* 92:322–331
- Cohen JD, Deeming J (1985) The national fire danger rating system: basic equations. US Forest Service technical report PSW-82. Pacific Southwest Forest Range Experimental Station, Berkeley, California, USA
- Dinku T, Ceccato P, Grover-Kopec E, Lemma M, Connor SJ, Ropelewski CF (2007) Validation of satellite rainfall products over East Africa's complex topography. *Int J Remote Sens* 28: 1503–1526
- Ebert EE (2005) Satellite versus model rainfall—Which one to use? Fifth international scientific conference on the global energy and water cycle, Orange County. Global Energy and Water Experiment. [http://www.gewex.org/5thConfposterT6-7\\_Ebert.pdf](http://www.gewex.org/5thConfposterT6-7_Ebert.pdf). Accessed 9 Mar 2009
- Fosberg MA (1971) Moisture content calculations for the 100-h timelag fuel in fire danger rating. US Department of Agriculture Forest Service Research Note RM-199. US Department of Agriculture Forest Service, Rocky Mountain Forest and Range Experiment Station, Fort Collins, Colorado, USA
- Fosberg MA (1977) Forecasting the 10-h timelag fuel moisture. USDA Forest Service research paper RM-187. Rocky Mountain Forest and Range Experiment Station, Fort Collins, Colorado, USA
- Fosberg MA, Rothermel RC, Andrews PL (1981) Moisture content calculations for 1,000-h timelag fuels. *For Sci* 27:19–26
- GADSC (2013) Autonomous government of the Department of Santa Cruz in partnership with FAN implements climate change program. Webpage of the Gobierno Autónomo Departamental de Santa Cruz (GADSC), Bolivia. <http://www.santacruz.gob.bo/turistica/medioambiente/cambioclimatico/contenido.php?IdNoticia=3409&IdMenu=30044>. Accessed 30 Jan 2013
- Goetz SJ, Prince SD, Goward SN, Thawley MM, Small J, Johnston A (1999) Mapping net primary production and related biophysical variables with remote sensing: applications to the Boreas region. *J Geophys Res* 104:27,719–727,734
- Goetz SJ, Bunn AG, Fiske GJ, Houghton RA (2005) Satellite-observed photosynthetic trend across boreal North America associated with climate and fire-disturbance. *Proc Natl Acad Sci* 102:13521–13525
- Grégoire JM, Tansey K, Silva JMM (2003) The GBA2000 initiative: developing a global burned area database from SPOT-VEGETATION imagery. *Int J Remote Sens* 24:1369–1376
- Hansen M, DeFries RS, Townshend JRG, Carroll M, Dimiceli C, Sohlberg RA (2003) Global percent tree cover at a spatial resolution of 500 meters: first results of the MODIS vegetation continuous fields algorithm. *Earth Interact* 7:1–15
- Heinsch FA, Andrews PL (2010) BehavePlus fire modeling system, version 5.0: Design and features. General technical report RMRS-GTR-249. Fort Collins: US Department of Agriculture, Forest Service, Rocky Mountain Research Station. (10,487 KB; p 111)
- Hirpa FA, Gebremichael M (2010) Evaluation of high-resolution Satellite precipitation products over very complex terrain in Ethiopia. *J Appl Meteorol Climatol* 29:1044–1051
- Huffman GJ, Adler RF, Bolvin DT, Gu G, Nelkin EF, Bowman KP, Hong Y, Stocker EF, Wolff DB (2007) The TRMM multisatellite precipitation analysis (TMPA): quasi-global, multiyear, combined-sensor precipitation estimates at fine scales. *J Hydrometeorol* 8:38–55
- Illera P, Fernández A, Delgado JA (1996) Temporal evolution of the NDVI as an indicator of forest fire danger. *Int J Remote Sens* 5(17):1093–1105
- INPE (2013) Fire Monitoring Program, Instituto Nacional de Pesquisas Espaciais, Brazil. <http://pirandira.cptec.inpe.br/queimadas/#>. Accessed 23 Jan 2013
- INPE-Instituto Nacional de Pesquisas Espaciais (2011) Portal do Monitoramento de Queimadas e Incêndios. Disponível em. <http://www.inpe.br/queimadas>. Accessed 30 Nov 2011
- Justice CO, Giglio L, Korontzi S, Owens J, Morisette JT, Roy D, Descloitres J, Alleaume S, Petitcolin F, Kaufman Y (2002) The MODIS fire products. *Remote Sens Environ* 83:244–262
- Katsanos D, Lagouvardos K, Kotroni V, Huffman GJ (2004) Statistical evaluation of MPA-RT high-resolution precipitation estimates from satellite platforms over the central and eastern Mediterranean. *Geophys Res Lett* 31:L06116. doi:10.1029/2003GL019142
- Keetch J, Byram GM (1968) A drought index for forest fire control. USDA Forest Service research paper SE-38. US Department of Agriculture-Forest Service, Asheville, NC, USA
- Killeen TJ, Chavez E, Peña-Claros M, Toledo M, Arroy L, Caballero J, Correa L, Guillén R, Quevedo R, Saldias M, Soria L, Uslar Y, Vargas I, Steininger M (2006) The Chiquitano dry forest, the transition between humid and dry forest in Eastern lowland Bolivia. In: Pennington T, Lewis GP, Ratter JA (eds) Neotropical savannas and dry forests: plant diversity, biogeography and conservation. Taylor & Francis, London, p 213–234
- Kummerow C, Simpson J, Thiele O, Barnes W, Chang ATC, Stocker E, Adler RF, Hou A, Kakar R, Wentz F, Ashcroft P, Kozi T, Hong Y, Okamoto I, Iguchi T, Kuroiwa H, Im E, Haddad Z, Huffman G, Ferrier B, Olson WS, Zipser E, Smith EA, Wilheit TT, North G, Krishnamurti T, Nakamura K (2000) The status of the tropical rainfall measuring mission (TRMM) after 2 years in orbit. *J Appl Meteorol* 39:1965–1982
- Lewis SL, Brando PM, Phillips OL, van der Heijden GMF, Nepstad D (2011) The 2010 Amazon drought. *Science* 331:554
- Machado, LAT, Ceballos J (2000) Satellite based products for monitoring weather in South America: winds and trajectories. 5th international winds workshop, Saanenmoser
- Matson M, Holben B (1987) Satellite detection of tropical burning in Brazil. *Int J Remote Sens* 8:509–516
- Monteith JL, Unsworth MH (1990) Principles of environmental physics, 2nd edn. Edward Arnold Publishers, New York
- Myneni RB, Hoffman S, Knyazikhin Y, Privette JL, Glassy J, Tian Y, Wang Y, Song X, Zhang Y, Smith GR, Lotsche A, Friedl M, Morisette JT, Votava P, Nemani RR, Running SW (2002) Global products of vegetation leaf area and fraction absorbed PAR from year one of MODIS data. *Remote Sens Environ* 83:214–231
- Nepstad D, Lefebvre P, da Silva UL, Tomasella J, Schlesinger P, Solorzano L, Moutinho P, Ray D, Benito JG (2004) Amazon drought and its implications for forest flammability and tree growth: a basin-wide analysis. *Glob Change Biol* 10:704–717
- NWCG (2013) National wildfire coordinating group (NWCG), Glossary of wildland fire terminology. <http://www.nwcg.gov/pms/pubs/glossary/f.htm>. Accessed 30 Jan 2013
- Onset (2012) <http://www.onsetcomp.com/products>. Accessed 20 Feb 2012
- Palmer WC (1965) Meteorological drought. US Department of Commerce research paper no. 45. US government printing office, Washington, DC, USA
- Phillips OL, Aragão LEOC, Lewis SL, Fisher JB, Lloyd J, López-González G, Malhi Y et al (2009) Drought sensitivity of the Amazon rainforest. *Science* 323:1344–1347
- Prince SD, Goward SN (1995) Global primary production: a remote sensing approach. *J Biogeogr* 22:815–835

- Rainwise (2012) [http://www.rainwise.com/products/index.php?Category=Rain\\_Gauges:Wired](http://www.rainwise.com/products/index.php?Category=Rain_Gauges:Wired). Accessed 20 Feb 2012
- Ray D, Nepstad D, Moutinho P (2005) Micrometeorological and canopy controls of fire susceptibility in a forested amazon landscape. *Ecol Appl* 15:1664–1678
- Roy DP, Lewis PE, Justice CO (2002) Burned area mapping using multi-temporal moderate spatial resolution data- a bi-directional reflectance mode-based expectation approach. *Remote Sens Environ* 83:263–286
- Running SW, Nemani RR, Heinsch FA, Zhao M, Reeves M, Hashimoto H (2004) A continuous satellite-derived measure of global terrestrial primary production. *Bioscience* 56:547–560
- Schroeder MJ (1969) Ignition probability. Office report 2106-1. US Department of Agriculture Forest Service, Rocky Mountain Forest and Range Experiment Station, Fort Collins, Colorado, USA
- Scott JH, Burgan RE (2005) Standard fire behavior fuel models: a comprehensive set for use with Rothermel's surface fire spread model. General technical report RMRS-GTR-153. US Department of Agriculture Forest Service, Rocky Mountain Forest and Range Experiment Station, Fort Collins, Colorado, USA
- Seemann SW, Li J, Menzel WP, Gumley LE (2003) Operational retrieval of atmospheric temperature, moisture, and ozone from MODIS infrared radiances. *J Appl Meteorol* 42:1072–1091
- Seemann SW, Borbas EE, Li J, Menzel WP, Gumley LE (2006) MODIS atmospheric profile retrieval algorithm theoretical basis document version 6. [http://modis.gsfc.nasa.gov/data/atbd/atbd\\_mod07.pdf](http://modis.gsfc.nasa.gov/data/atbd/atbd_mod07.pdf). Accessed 1 Jun 2009
- Setzer AW, Sismanoglu RA (2009) Fire risk: summary of calculations. INPE. [http://www.cptec.inpe.br/queimadas/documentos/doc\\_RF\\_2007.pdf](http://www.cptec.inpe.br/queimadas/documentos/doc_RF_2007.pdf). Accessed 9 Apr 2009
- USFS (2013) US Forest Service Wildland Fire Assessment System. <http://www.wfas.net>. Accessed 23 Jan 2013
- USGS (2004) Shuttle radar topography mission, 3 arc second scene SRTM\_u03\_n008e004, Unfilled Unfinished 2.0, Global Land Cover Facility, University of Maryland, College Park, Maryland, February 2000
- Wan Z (2009) MODIS land surface temperature products users' guide. [http://www.icesc.ucsb.edu/modis/LstUsrGuide/MODIS\\_LST\\_products\\_Users\\_guide.pdf](http://www.icesc.ucsb.edu/modis/LstUsrGuide/MODIS_LST_products_Users_guide.pdf). Accessed 6 Apr 2009
- Wan Z, Li Z-L (1997) A physics-based algorithm for retrieving land-surface emissivity and temperature from EOS/MODIS data. *IEEE Trans Geosci Remote Sens* 35:980–996
- Wan Z, Zhang Y, Zhang Q, Li Z-L (2004) Quality assessment and validation of the MODIS global land surface temperature. *Int J Remote Sens* 25:261–274
- Wang J, Wolff DB (2010) Evaluation of TRMM ground-validation radar-rain errors using rain gauge measurements. *J Appl Meteorol Climatol* 49:310–324
- Wang W, Liang S, Meyers T (2007) MODIS land surface temperature products using long-term nighttime ground measurements. *Remote Sens Environ* 112:623–635